

The role of an intense jet in the Tsugaru Strait in the formation of the outflow gyre revealed using high-frequency radar data

Hitoshi Kaneko^{1,1}, Ken'ichi Sasaki^{1,1}, Hiroto Abe^{2,2}, Shuichi Watanabe^{1,1}, and Yoshiaki Sato^{1,1}

¹Mutsu Institute for Oceanography

²Faculty of Fisheries Sciences

November 30, 2022

Abstract

The seasonal pattern of the eastward jet through the Tsugaru Strait between 2014 and 2019 was investigated using surface velocity data obtained from high-frequency radar located in the eastern part of the strait. The vorticity-front-model was used to estimate the volume transport of low-vorticity water and the intensity of the vorticity gap at the front using the climatological mean zonal velocity distribution. The flow mode at the outlet was then defined as either the summer/autumn “gyre mode” or winter/spring “coastal mode”. The distribution of the parameters was consistent with the theoretical understanding, showing that in addition to the volume transport, an increase in the vorticity gap can also contribute to the development of the gyre. The results also suggest an impact from the jet in the strait on the coastal flow along the coast of Japan.

1 **The role of an intense jet in the Tsugaru Strait in the formation of the outflow gyre**
2 **revealed using high-frequency radar data**

3
4 **H. Kaneko¹, K. Sasaki¹, H. Abe^{1,2}, S. Watanabe¹, and Y. Sato¹**

5
6 ¹ Mutsu Institute for Oceanography, Research Institute for Global Change, Japan Agency for
7 Marine-Earth Science and Technology, Mutsu, Japan.

8 ² Faculty of Fisheries Sciences, Hokkaido University, Hakodate, Japan.

9
10 Corresponding author: Hitoshi Kaneko (h_kaneko@jamstec.go.jp)

11
12 **Key Points:**

- 13 • Observational verification of the seasonal flow pattern theory of the Tsugaru Warm
14 Current based on velocity data from high-frequency radar
- 15 • Importance of vorticity gap at the front of the jet recognized in addition to the volume
16 transport of the current on the flow pattern change
- 17 • Effectiveness of high-frequency radar with diagnostic scheme improves understanding of
18 the role of the strait in coastal flow around Japan
19

20 **Abstract**

21 The seasonal pattern of the eastward jet through the Tsugaru Strait between 2014 and 2019 was
22 investigated using surface velocity data obtained from high-frequency radar located in the
23 eastern part of the strait. The vorticity-front-model was used to estimate the volume transport of
24 low-vorticity water and the intensity of the vorticity gap at the front using the climatological
25 mean zonal velocity distribution. The flow mode at the outlet was then defined as either the
26 summer/autumn “gyre mode” or winter/spring “coastal mode”. The distribution of the
27 parameters was consistent with the theoretical understanding, showing that in addition to the
28 volume transport, an increase in the vorticity gap can also contribute to the development of the
29 gyre. The results also suggest an impact from the jet in the strait on the coastal flow along the
30 coast of Japan.

31

32 **Plain Language Summary**

33 The Tsugaru Warm Current forms part of the coastal flow around Japan and shows remarkable
34 seasonal changes in its flow pattern, which are similar to the Kuroshio meandering. The current
35 flows along the coast from winter to spring, but demonstrates large anticyclonic meandering in
36 the offshore direction, known as “gyre mode”, from summer to autumn. The cause of this change
37 in the flow pattern has been thought to be the seasonal change in volume transport. In this study,
38 we used high-resolution temporal and spatial data obtained from a high-frequency radar system,
39 as well as the relationship between coastal waves and offshore jets with fronts, to identify
40 another important factor that affects the seasonal flow pattern of the current, namely, “vorticity”.
41 Our results demonstrate the applicability and effectiveness of the high-frequency radar
42 monitoring, and that it could be successfully used in other coastal regions, including other parts

43 of the same strait. Moreover, our study indicates that the response of the flow in the strait to
44 volume transport and vorticity will be important to long-term changes in the wider circulation in
45 relation to global warming and decadal-scale changes.

46

47 **1 Introduction**

48 The Tsugaru Strait is located between the mainland of Japan (Honshu) and Hokkaido
49 (Figure 1a). The Tsugaru Warm Current (TWC; Figure 1a) is a branch of the Tsushima Warm
50 Current, which itself has origins in the Kuroshio southwest of Kyushu island as well as the flow
51 from the Taiwan Strait (Isobe, 1999). The other branch flows north along the coast of Hokkaido
52 as the Soya Warm Current. These currents are closely related and can be considered one system
53 (e.g., Kida et al., 2016). In the Tsugaru Strait, a recent study (Wakita et al., submitted to GRL)
54 reported faster acidification than that in the global ocean. In addition, a far more intense vertical
55 mixing than in the open ocean, and enhancement of vertical nitrate transport above the
56 characteristic topography in the western part of the strait were also observed (Tanaka et al.,
57 2021). These recent studies suggest these characteristic phenomena that occur in the strait could
58 affect a wider region via the TWC.

59 The mean volume transport of the TWC and its seasonal variations have been estimated
60 as 1.5 ± 0.3 Sv, ($=10^6$ m³ s⁻¹; e.g., Onishi and Ohtani, 1997; Nishida et al., 2003). Based on the
61 sea level difference between Fukaura and Hakodate (Figure 1b), Nishida et al. (2003) also
62 reported that the transport increases from spring to summer (maximum in July and August) and
63 decreases from autumn to winter (minimum in February). As another seasonal variation, there is
64 a remarkable change in the outflow pattern of the TWC from the eastern outlet of the strait. This
65 outflow switches from “coastal mode”, which is a nearshore flow along the coast of the
66 Shimokita Peninsula (in winter and spring), to “gyre mode”, which is a large anticyclonic gyre
67 that develops south of Hokkaido (in summer and autumn) (e.g., Conlon, 1982; Figure 1b). It is
68 thought that the increase in volume transport through the strait could initiate the development of
69 the gyre mode (e.g., Kawasaki and Sugimoto, 1988).

70 In addition to the volume transport, Kubokawa (1991; hereafter K91) raised another
71 important aspect of the difference in the vorticity across the jet based on the reduced gravity
72 model with vorticity-front (Figure S1). Using parameters such as the transport of water with a
73 relatively lower potential vorticity between the front and the boundary (area A in Figure S1), the
74 vorticity gap at the front, and the total volume transport at the outflow, K91 revealed that an
75 enhancement of the vorticity gap relative to the total volume transport is important for the
76 transition from “coastal” to “gyre” mode, in addition to an exceeding of the volume transport of
77 the lower potential vorticity fluid at the outlet of the strait relative to that at the far downstream
78 region. Although Nof and Pichevin (1999) proposed that the Tsugaru and the Alboran gyres
79 could develop regardless of the initial vorticity, and they also commented on the importance of
80 on-site estimation of vorticity in the currents as a subject for future investigation.

81 However, because of the lack of temporal and spatial observations from vessels and
82 moorings, the importance of the vorticity associated with the jet remains to be fully clarified.
83 This lack of observational data arises because it is difficult to estimate the mean geostrophic field
84 from time-limited shipboard current measurements, such as those made using acoustic Doppler
85 current profilers, because of the strong tidal current in the strait (Isoda and Baba, 1998; Onishi et
86 al., 2004; Luu et al., 2011; Ohta et al., 2014; Yamaguchi et al., 2020; Matsuura and Isoda, 2020).
87 The use of multiple moorings across the jet is also difficult due to the intense velocity and
88 frequent ship traffic through the strait. Moreover, although satellite observations can provide
89 gridded time series data covering a long period, the spatial resolution with respect to velocity is
90 too coarse for vorticity analysis.

91 Therefore, in this study, we used high-frequency radar (HFR) for surface current
92 monitoring in the eastern part of the strait (Figure 1c). This system can provide suitably high-

93 resolution spatial data, and also long-term and homogeneously (equally spaced in time)
94 continuous data that allowed us to estimate the background quasi-geostrophic current distribution
95 for the vorticity analysis. Using the data obtained by the HFR system developed by the Mutsu
96 Institute for Oceanography (MIO), Japan Agency for Marine-Earth Science and Technology
97 (JAMSTEC), we confirmed the effect of the vorticity gap at the jet axis based on the diagram
98 proposed by K91. Our results, which are in good agreement with the theory of K91, will be
99 presented below, after a brief explanation of our data analysis methods and the theory described
100 in K91. Moreover, the role of the eastern part of the strait will be discussed from the point of
101 view of the island circulation along the coast, which might be a contributor to the long-term
102 variations and/or rapid shifts in environmental conditions.

103

104 **2 Materials and Methods**

105 Surface velocity data for the eastern Tsugaru Strait were obtained from the MIO ocean
106 radar data site (MORSETS; <https://www.godac.jamstec.go.jp/morsets/e/top/>). The monitoring
107 system comprises three high-frequency radars (SeaSonde, 13.9 MHz, CODAR Ocean Sensors)
108 located in the Tsugaru Strait: two on the Shimokita Peninsula and the other on Hokkaido (Figure
109 1c). The system yields velocity distributions with a horizontal resolution of approximately 3 km
110 every 30 minutes, and the same system has also been used to monitor the Tsushima Warm
111 Current (e.g., Yoshikawa et al., 2006). We used data covering the period between March 2014,
112 when observations began, and December 2019. Data were collected from within the region
113 bounded by 140.93–141.98°E and 41.38–42.05°N (Figure 1c).

114 To investigate seasonal changes in the mean velocity field, we estimated the
 115 climatological mean of zonal velocity, U , with respect to a series of 5-km zonal bands, which
 116 were set from 140.92°E to 142.04°E with a half-overlap (Figure 1c). Within this zone, the
 117 climatological mean was estimated each day from January 1st to December 31st over the period
 118 2014–2019, using a width of 10 days. Outliers were excluded if they had a value that fell outside
 119 of three standard deviations from the mean. Examples of the seasonal variation of U are shown
 120 in Figure 2a and b. The axis of the jet was defined as the latitude of the U -maximum (extremum).
 121 In addition, the meridional distribution of U was used to estimate the ratio of the vorticity gap at
 122 the front to the total volume transport at the outflow through calculation of the difference in U
 123 and its accumulation (integration) from the northern boundary of the grid, as described below.
 124 Before that, the parts of K91 relevant to the present study will be briefly introduced.

125 Under conditions of stratification with a deep and passive lower layer, together with a
 126 small Rossby number, $\varepsilon \ll 1$, and using the governing equations of the upper layer without
 127 viscosity and diffusion, K91 set the geostrophic stream function with respect to the second order
 128 term, $O(\varepsilon)$, along the north–south section at the outlet of the strait as follows.

$$129 \quad \psi_{(\alpha)} = \begin{cases} 0 & \text{for } \alpha \leq -w \\ \frac{h_0 + P\{\cosh l - 1\}}{\sinh w} \sinh(\alpha + w) & \text{for } -w < \alpha < 0 \\ h_0 & \text{for } \alpha \geq 0 \end{cases}$$

$$130 \quad - \begin{cases} 0 & \text{for } -w < \alpha \leq -l, \\ P\{\cosh(\alpha + l) - 1\} & \text{for } -l < \alpha \leq 0, \end{cases} \quad (1)$$

131 Here, α denotes the north–south direction (southward positive), $\alpha = 0$ indicates the
 132 southern edge of the strait (Figure S1), and w is the width of the strait. In addition, h_0 represents
 133 the total volume transport of the outflow, and P represents the gap in vorticity at the front, that is,

134 with respect to the distribution of the potential vorticity, q , along the section at the outlet, which
 135 we defined as (Figure S1):

$$136 \quad q = \nabla^2 \psi - \psi = \begin{cases} -P & \text{for } -l \leq \alpha < 0, \\ 0 & \text{for } -w < \alpha < -l, \end{cases} \quad (2)$$

137 The ratio of the volume transport of the low potential vorticity fluid ($q = -P, P > 0$) to the
 138 total volume transport Q_R can be written as follows:

$$139 \quad Q_R = 1 - \psi_{(-l)}/h_0, \quad (3)$$

140 On the other hand, K91 set the distribution of the stream function in the β (west–east)
 141 direction in the downstream region ($\alpha \rightarrow \infty$) as follows:

$$142 \quad \psi_{(\beta)} = \{h_0 + P(\cosh L - 1)\}e^{-\beta}$$

$$143 \quad - \begin{cases} P\{\cosh(L - \beta) - 1\} & \text{for } \beta < L, \\ 0 & \text{for } \beta \geq L, \end{cases} \quad (4)$$

144 where L is the front location from the western boundary (Figure S1). The ratio of the
 145 transport of the low potential vorticity fluid to the total transport there, Q_{Rc} , can be written as
 146 follows:

$$147 \quad Q_{Rc} = \begin{cases} 1 - P/2h_0 & \text{for } P/h_0 < 1, \\ h_0/2P & \text{for } P/h_0 \geq 1, \end{cases} \quad (5)$$

148 Then, following Stern (1986), K91 provided the condition regarding the propagating
 149 direction of the long frontal wave using the parameters referred to above:

$$150 \quad c = \{h_0 - P(1 - e^{-L})\}e^{-L}, \quad (6)$$

151 where, c is the propagating speed of the long frontal wave. Thus, when c is negative, the
 152 wave propagates upstream. Using this condition, K91 defined three domains in the P/h_0 – Q_R

153 plane as a diagnostic diagram for the flow pattern: (I) a steady coastal mode with $Q_R < Q_{Rc}$, (II) a
 154 widening coastal mode with $Q_R > Q_{Rc}$ and $P/h_0 < 1$, and (III) a gyre mode with $Q_R > Q_{Rc}$ and
 155 $P/h_0 \geq 1$. We applied this diagnostic diagram to the parameters estimated from the surface
 156 velocity data obtained from MORSETS.

157 First, we estimated the ratio of the volume transport of the low potential vorticity fluid to
 158 the total volume transport along the outlet of the strait, Q_R . We defined the accumulation of the
 159 climatological mean of the zonal velocity from the northern boundary as ψ' , assuming that ψ' at
 160 the northern boundary was zero. The accumulations at the axis of the jet and the southern coastal
 161 boundary or boundary of the HFR observation (Figure 1c) were defined as $\psi'_{(-l)}$ and h_0' ,
 162 respectively. Then, equivalent Q_R' was defined as:

$$163 \quad Q_R' = 1 - \psi'_{(-l)}/h_0', (7)$$

164 Here, we assumed that $\psi'_{(-l)}/h_0'$ was equivalent to $\psi_{(-l)}/h_0$ as defined by K91.

165 Second, we estimated the ratio of the gap in the vorticity at the front to the total volume
 166 transport, P'/h_0' , as follows. The difference in the zonal velocity, $\psi'_{\alpha\alpha}$, was calculated as the
 167 representation of the second derivative of the geostrophic stream function. The locations of the
 168 maximum and minimum of $\psi'_{\alpha\alpha}$ were defined as α_1 and α_2 (Figure 2c and d). When the multiple
 169 maxima were obtained, especially in winter, we defined the location of the northern maximum as
 170 α_1 and the adjacent southern minimum as α_2 (Figure 2d), because the southern coastal mode of
 171 the TWC in winter has larger Rossby number (>0.4) than that of the northern coastal mode
 172 (<0.4 ; T. Yasui, personal communication, 2021). Then, in the present study, the equivalent gap
 173 in the vorticity at the front, P' , was estimated using observed gap, $\psi'_{\alpha\alpha(\alpha_1)} - \psi'_{\alpha\alpha(\alpha_2)}$, as follows:

$$174 \quad P' = \psi'_{(-l)} \times \left(\psi'_{\alpha\alpha(\alpha_1)} - \psi'_{\alpha\alpha(\alpha_2)} \right) / \psi'_{\alpha\alpha(\alpha_1)}, \quad (8)$$

175 Assuming that $P'/h_0' = P/h_0$, we used P'/h_0' as another parameter in the diagnosis. Then,
176 the maximum value of the ratio of the volume transport of the low potential vorticity fluid to the
177 total volume transport in the far downstream region, Q_{Rc}' , was defined following K91.

178 Using the parameters Q_R' , Q_{Rc}' , and P'/h_0' , we investigated the flow pattern of TWC
179 based on the diagram suggested by K91. The index of the flow pattern (coastal or gyre) was
180 defined using the intensity of the meridional velocity at the outlet of the strait. The climatological
181 mean of the meridional velocity in each bin (Figure 1c), V (northward positive), was calculated.
182 Then, the meridional average of the velocity over the area 41.51–41.67°N was calculated in each
183 bin located between 141.42°E and 141.63°E for each day as $\langle V \rangle_{41.51-41.67^\circ N}$. Seasonal changes in
184 the meridional velocity at the outlet of the strait are shown in the Results and Figure 3. Then, the
185 zonal mean (141.42–141.63°E for Q_R' , Q_{Rc}' , and P'/h_0' , and 141.54–142.04°E for
186 $\langle V \rangle_{41.51-41.67^\circ N}$) was calculated again to plot the parameters on the Q_R – P/h_0 plane, and we
187 diagnosed the flow pattern by comparing it with the meridional velocity at the outlet (Figure 4).

188

189 **3 Results**

190 The seasonal distribution of U across the strait at 141.29–141.38°E (Region-a) and at
191 141.50–141.58°E (Region-b) are shown as examples in Figure 2a and b, respectively. Both
192 figures indicate a northward shift of the eastward jet, and an opposite westward flow to the south
193 of the jet in summer, implying the occurrence of an anticyclonic flow structure south of the jet.
194 In Region-b, U shows a bimodal distribution, with a stronger coastal peak and the other a weaker
195 enhancement in the center of the strait (41.7–41.8°N, Figure 2b). Whereas the intensity of U
196 around the axis increased during summer in Region-a, in Region-b, U near the coast increased

197 during winter (Figure 2b). In other words, our results suggest the disappearance of the near-coast
198 eastward current at the outlet in summer. This seasonal shift of the jet axis within the strait was
199 consistent with that reported by Abe et al. (2020).

200 The distribution of $\psi'_{\alpha\alpha}$ also showed a clear seasonal variation (Figure 2c and d)
201 associated with that of U . An increase in the vorticity gap across the front coincident with the
202 axis was recognized in summer. This was especially evident in Region-b, where the spring–
203 summer bimodal distribution was replaced by a well-defined single maximum to the north of the
204 jet axis, and a clear minimum near the southern boundary of the vorticity (Figure 2d).

205 Consequently, the large gap between the pair was estimated at the outlet of the strait as a
206 result of the enhanced single-peak jet having a spatial scale similar to that of the width of the
207 strait. On the other hand, h_0' calculated as an accumulation of U along the meridional direction,
208 also showed an increase in summer, especially in Region-a (Figure 2c). Thus, as a next step, we
209 calculated the ratio of P' to h_0' for each climatological day from January 1st to December 31st,
210 and compared its spatio-temporal plot with that of Q_R' .

211 The seasonal variation of P'/h_0' showed clear intensification during the summer, reaching
212 a value of 2.5 (Figure 3a). This seasonal contrast in P'/h_0' was especially remarkable in the
213 region above the Shiriya Spur (141.4–141.6°E, Figure S2). The maximum value of 2.5 occurred
214 in August in this region, and from June to November it was generally greater than 1. In contrast,
215 after November, P'/h_0' decreased rapidly to less than 1. In addition to the high value of P'/h_0'
216 during summer, Q_R' also showed a relatively large value (0.3–0.5) between June and November,
217 although Q_R' temporarily became smaller than 0.3 in August when P'/h_0' reached its maximum.
218 The meridional velocity in the region of the outlet showed the development of northward
219 velocity from June to the middle of August, and this continued until November (Figure 3b). The

220 peak date of P'/h_0' corresponded with that of the northward velocity (mid-August). Thus, we
221 suggest that the gyre develops from June to mid-August under the high P'/h_0' conditions. The
222 maintenance of the gyre is also implied until November under conditions of $P'/h_0' = 1.0-1.5$ and
223 $Q_R' = 0.3-0.5$, which is consistent with the findings of previous studies (e.g., Conlon, 1982;
224 Rosa et al., 2007). In the upstream region of $141.1-141.4^\circ\text{E}$, although P'/h_0' generally exceeded
225 1 throughout year, Q_R' remained below 0.3, except during summer, which implies that the
226 conditions required for gyre development were also established during the summer (Figure 3a).

227 Next, to compare the result obtained from our HFR observations with the theory
228 suggested by K91, we calculated the zonal mean of P'/h_0' and Q_R' over the region $141.42-$
229 141.63°E , at just the outlet of the strait (Figures 3 and S2). After that, each parameter was plotted
230 on the diagnostic diagram proposed by K91 using a color scale to indicate the meridional
231 velocity at the outlet (Figure 4). The result was clearly consistent with K91; i.e., the dots located
232 in the gyre (coastal) mode region showed an intense northward (southward) current at the outlet
233 of the strait. Although an increase in Q_R' to $0.3-0.5$, together with a P'/h_0' value of slightly less
234 than 1, were evident in spring (April–June), the current direction around the outlet of the strait
235 was towards the south, suggesting that the gyre does not develop under these conditions. In
236 contrast, although Q_R' showed a constant value of approximately 0.3 during the summer (July–
237 September), the northward current around the outlet was indicated by the large value of P'/h_0'
238 (>1.5).

239

240 **4 Discussion**

241 Our results are consistent with the theory proposed by K91 (Figure 4). Therefore, the
242 importance of the vorticity gap at the front (the axis of the TWC) as a factor in gyre formation
243 (in addition to the volume transport of the TWC) has been confirmed again using our
244 observational data obtained from the HFR. With respect to the annual data, the distribution of
245 each parameter in the diagnostic diagram was similar to that of the six-year climatological data,
246 although there were exceptions. Consequently, we conclude that our results support the
247 reliability and effectiveness of using high-resolution HFR observations with the diagnostic
248 scheme, and also its applicability to other coastal regions such as the Alboran Sea. However,
249 note that the TWC shows large seasonal variability in stratification (e.g., Sugimoto and
250 Kawasaki, 1984), and this kind of diagnostic approach should be treated with caution, especially
251 in winter when the stratification is weaker.

252 To test our HFR approach, we also applied it to an upstream region of the same strait
253 (Figure S3). One of the notable characteristics of the seasonal changes in the flow within the
254 upper section of the strait during summer was the disappearance of the coastal eastward current
255 at the outlet and the northward shift of the flow, which had only a single axis (Figure 2b). This
256 caused the sharp single peak in the jet and the large vorticity gap at the front, which contributed
257 to the mode change. The cause of the disappearance and shift in the flow remains one of the
258 issues to be addressed. The application of the theory of outflow from the strait may be
259 reasonable, because the coastline of the peninsula extends southwards in the region east of
260 141.1 °E (Figure S3a). Thus, frontal wave stagnation there may occur as another sub-gyre in the
261 region. In fact, in summer, negative vorticity development related to the meridional velocity was
262 evident around 141.2–141.4°E (Figure S3b) in association with the high P/h_0 conditions in the

263 region 141–141.2°E (Figure S3c). Development of the sub-gyre could push the axis to the north,
264 and weaken the downstream flow along the northern coast. Note that this approach in this
265 upstream region should be treated with caution, again, because the Rossby number in this region
266 would be larger than that in the outlet of the strait. Thus, investigations of the sub-gyre
267 development are ongoing based on the coastal monitoring networks of MORSETS. Moreover,
268 the cause of seasonal change in the jet form should also be examined in relation to other physical
269 processes, including water mass distribution, tides, and volume transport by the TWC itself
270 (which would be related to wind stress curl).

271 The modulation of TWC such as the developments of the gyres during summer, suggests
272 that the Tsugaru Strait has an important impact on the system of the currents along the Japanese
273 coast including the Tsushima Warm Current, and the Kuroshio. Kida et al. (2020) explained that
274 the increasing trend seen in the volume transport of the Tsushima Warm Current reflects the
275 long-term northward (coastward) shift of the Kuroshio axis. This interpretation was based on the
276 assumption that the integration of the horizontal frictional torque caused by the coastal flow
277 around the islands (including Honshu, Kyushu, and Shikoku; Figure 1a) should be zero under
278 steady-state conditions (Yang, 2007; Kida et al., 2016). The development of the gyre and the
279 associated offshore movement of the flow path in the Tsugaru Strait may affect the integration of
280 the horizontal frictional torque caused by the coastal flow. Thus, it will be worthwhile
281 investigating the role of the Tsugaru Strait more carefully in relation to the increasing trend in
282 the volume transport in the upstream region.

283 Moreover, the decadal variability of the circulation within the upstream region may cause
284 similar variations in the TWC. Kaneko et al. (2018) reported a shift in the Kuroshio axis along
285 141°N, which was synchronous with both a stable Kuroshio Extension and the Pacific Decadal

286 Oscillation, and this situation persisted for about 10 years after the 1998/1999 regime shift. If
287 such a synchronized shift of the axis could cause changes in the transport of the TWC, rapid
288 changes in biota synchronized with the shift might be caused along the warm currents around
289 Japan, including the TWC. Recently, the northward expansion of harmful dinoflagellates into the
290 strait, which can cause red tides, was reported, and transport by the TWC was suspected as one
291 of causes (Shimada et al., 2016). Therefore, in future, the role of the eastern part of the Tsugaru
292 Strait in the modulation of the flows should be clarified with respect to both long-term trends and
293 decadal variations, as this could have a large impact on the biota. Enlargement of HFR
294 observations, development of high-resolution numerical models, and enhancing the coastal
295 observation networks, including monitoring buoys, would all contribute to this task.

296

297 **Acknowledgments**

298 The The authors acknowledge the help of the staff of the Mutsu Institute for Oceanography and
299 the Research Institute for Global Change of JAMSTEC. The HFR data used in the present study
300 was distributed through MIO, JAMSTEC (<https://www.godac.jamstec.go.jp/morsets/e/top/>). We
301 sincerely acknowledge the technical support staff from Marine Work Japan. We also thank Dr.
302 M. Wakita, T. Yasui, S. Tatamisashi, T. Hashimukai, T. Nakayama, and S. In for their helpful
303 comments.

304

305 **References**

- 306 Abe, H., K. Sasaki, T. Yasui, and M. Wakita (2020) Observation of Tsugaru warm current by
307 High Frequency Radar and preliminary result for its prediction, *Kaiyo Monthly*, 52, 312–316. (in
308 Japanese)
- 309 Conlon, D. M. (1982), On the outflow modes of the Tsugaru Warm Current, *La mer*, 20, 60–64.
- 310 Isobe, A. (1999) On the origin of the Tsushima Warm Current and its seasonality. *Cont. Shelf*
311 *Res.*, 19 (1), 117–133. [https://doi.org/10.1016/S0278-4343\(98\)00065-X](https://doi.org/10.1016/S0278-4343(98)00065-X)
- 312 Isoda, Y., and K. Baba (1998), Tides and tidal currents in the Tsugaru strait. *Bull. Fac. Fish.*
313 *Hokkaido Univ.*, 49 (3), 117– 130 (in Japanese with English abstract)
- 314 Japan Agency for Marine-Earth Science and Technology MORSETS website (2020), MIO ocean
315 radar data site for Eastern Tsugaru Strait. <https://www.godac.jamstec.go.jp/morsets/e/top/>.
316 Accessed on 22 Nov. 2020

- 317 Kaneko, T. Okunishi, T. Seto, H. Kuroda, S. Itoh, S. Kouketsu, and D. Hasegawa (2018), Dual
318 effects of reversed winter–spring temperatures on year-to-year variation in the recruitment of
319 chub mackerel (*Scomber japonicus*), *Fish. Oceanogr.*, 28, 1–16,
320 <https://doi.org/10.1111/fog.12403>
- 321 Kawasaki, Y. and T. Sugimoto (1988), A laboratory study of the short-term variation of the
322 outflow pattern of the Tsugaru Warm Water with a change in its volume transport. *Bull. Tohoku*
323 *Reg. Fish. Res. Lab.*, 50, 203–215 (in Japanese with English abstract)
- 324 Kida, S., B. Qi, J. Yang, and X. Lin (2016) The annual cycle of the Japan Sea Throughflow. *J.*
325 *Phys. Oceanogr.*, 46 (1), 23–39, doi: 10.1175/JPO-D-15-0075.1
- 326 Kida, S., K. Takayama, Y. N. Sasaki, H. Matsuura, and N. Hirose (2020), Increasing trend in
327 Japan Sea Throughflow transport, *J. Oceanogr.*, <https://doi.org/10.1007/s10872-020-00563-5>
- 328 Kubokawa, A. (1991), On the behavior of outflows with low potential vorticity from a sea strait.
329 *Tellus A*, 43, 168–176. <https://doi.org/10.1034/j.1600-0870.1991.t01-1-00007.x>
- 330 Luu, Q. H., K. Ito, Y. Ishikawa, and T. Awaji (2011), Tidal transport through the Tsugaru Strait
331 — part I: Characteristics of the major tidal flow and its residual current. *Ocean Sci. J.*, 46, 273–
332 288. <https://doi.org/10.1007/s12601-011-0021-z>
- 333 Matsuura, H., and Y. Isoda (2020), Pseudo-fortnightly variation produced by interaction between
334 passage-flow and diurnal tidal currents in the Tsugaru Strait, *Bull. Fac. Fish. Hokkaido Univ.*, 70
335 (1), 13–23, doi:10.14943/bull.fish.70.1.13
- 336 Nishida, Y., I. Kanomata, I. Tanaka, S. Sato, S. Takahashi, and H. Matsubara (2003), Seasonal
337 and Interannual Variations of the Volume transport through the Tsugaru Strait. *Oceanogr. Jpn.*,
338 12 (5), 487–499, <https://doi.org/10.5928/kaiyou.12.487> (in Japanese with English abstract)
- 339 Nof, D., and T. Pichevin (1999) The Establishment of the Tsugaru and the Alboran Gyres. *J.*
340 *Phys. Oceanogr.*, 29(1), 39–54, DOI: [https://doi.org/10.1175/1520-](https://doi.org/10.1175/1520-0485(1999)029<0039:TEOTTA>2.0.CO;2)
341 [0485\(1999\)029<0039:TEOTTA>2.0.CO;2](https://doi.org/10.1175/1520-0485(1999)029<0039:TEOTTA>2.0.CO;2)
- 342 Onishi, M., and K. Ohtani (1997) Volume transport of the Tsushima Warm Current, west of
343 Tsugaru Strait bifurcation area. *J. Oceanogr.*, 53(1), 27–34,
- 344 Onishi M., Y. Isoda, H. Kuroda, M. Iwahashi, C. Saitoh, T. Nakayama, T. Ito, K. Iseda, K.
345 Nishizawa, S. Shima, and O. Togawa (2004), Winter Transport and Tidal Current in the Tsugaru
346 Strait. *Bull. Fac. Fish. Hokkaido Univ.*, 55 (2), 105–119.
- 347 Ohta, S., Y. Isoda, S. Yoshimura, K. Syouji, S. Arita, K. Kawano, X. Fang, and N. Kobayashi
348 (2014), Internal tidal waves generated over the sill topography in the Tsugaru Strait, *Sea and Sky*,
349 90 (5), 63–84, (in Japanese with English abstract)
- 350 Rosa, A. L., Y. Isoda, K. Uehara, and T. Aiki (2007), Seasonal Variations of Water System
351 Distribution and Flow Patterns in the Southern Sea Area of Hokkaido, Japan. *J. Oceanogr.*, 63,
352 573–588, doi:10.1007/s10872-007-0051-4.
- 353 Shimada, H., M. Kanamori, H. Yoshida, and I. Imai (2016), First record of red tide due to the
354 harmful dinoflagellate *Karenia mikimotoi* in Hakodate Bay, southern Hokkaido, in autumn,
355 2015. *Nippon Suisan Gakk.*, 82(6), 934–938, <https://doi.org/10.2331/suisan.16-00033>, (in
356 Japanese with English abstract)

- 357 Stern, M. E. (1986), On the amplification of convergences in coastal currents and the formation
 358 of “squirts”. *J. Mar. Res.*, 44 (3), 403–421, <https://doi.org/10.1357/002224086788403097>
- 359 Sugimoto, T., and Y. Kawasaki (1984) Seasonal and year-to- year variations of the Tsugaru
 360 Warm Current and their dynamical interpretation. *Bull. Coastal Oceanogr.*, 22, 1–11 (in
 361 Japanese).
- 362 Tanaka, T, H. Hasegawa, T. Okunishi, H. Kaneko, and T. Ono (2021), Internal Hydraulic Jump
 363 in the Tsugaru Strait, *J. Oceanogr.* <https://doi.org/10.1007/s10872-020-00588-w>
- 364 Yamaguchi, T., Y. Isoda, U. Itoh, T. Mukai, and N. Kobayashi (2020), Observation and model
 365 experiments on an internal-wave packet accompanied by streak bands over the sill topography of
 366 Tsugaru Strait, *Oceanogr. Jpn*, 29 (3), 71–90, https://doi.org/10.5928/kaiyou.29.3_71 (in
 367 Japanese with English abstract)
- 368 Yang, J. (2007), An oceanic current against the wind: how does Taiwan Island steer warm water
 369 into the East China Sea? *J. Phys. Oceanogr.*, 37 (10) 2563–2569, doi: 10.1175/JPO3134.1
- 370 Yoshikawa, Y., A. Masuda, K. Marubayashi, M. Ishibashi, and A. Okuno (2006), On the
 371 accuracy of HF radar measurement in the Tsushima Strait, *J. Geophys. Res.*, 111, C04009,
 372 doi:10.1029/2005JC003232.

373

374

375 **Figure captions**

376 **Figure 1.** (a) Schematic diagram of the flows around Japan. (b) Seasonal flow pattern of the
 377 Tsugaru Warm Current. (c) Observation site of the present study and distribution of the temporal
 378 mean velocity at each grid point. The square grids in (c) indicate the bins used to calculate the
 379 zonal average of the zonal velocity.

380 **Figure 2.** Examples of date–latitude plots of (a) and (b) zonal velocity, and (c) and (d) ψ' (thin
 381 lines) and $\psi'_{\alpha\alpha}$ (color and thick lines). The left (right) column denotes Region-a (Region-b). The
 382 black line in (a) and (b) denotes the latitude of the jet axis. The orange (blue) line in (c) and (d)
 383 denotes the latitude of the maximum (minimum) of $\psi'_{\alpha\alpha}$. See text for definitions of ψ' and $\psi'_{\alpha\alpha}$.

384 **Figure 3.** Longitude–date plot of (a) Q_R' (color) and P'/h_0' (contours), and (b) meridional
 385 velocity averaged in north–south band. See text for definitions of Q_R' , P' , and h_0' .

386 **Figure 4.** The diagnostic diagram for the flow pattern.

387

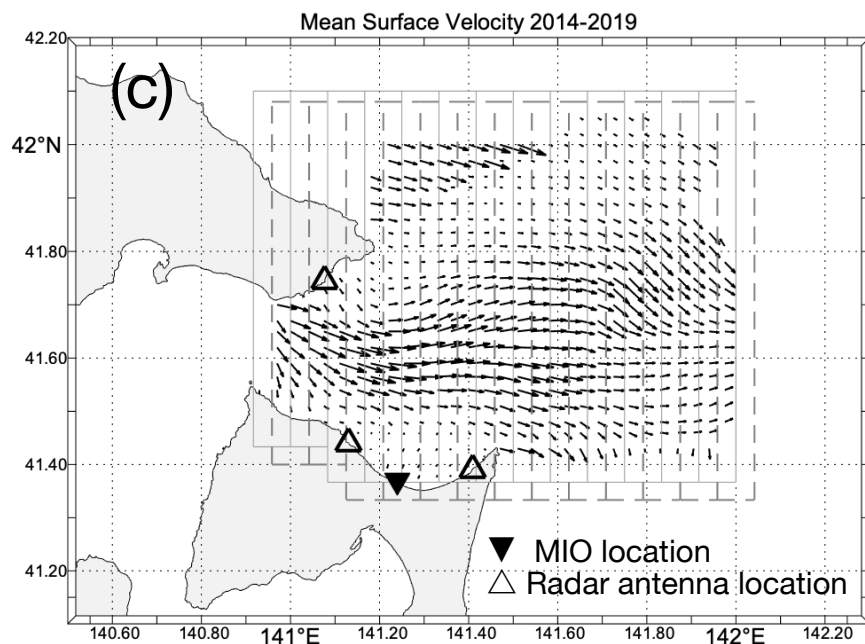
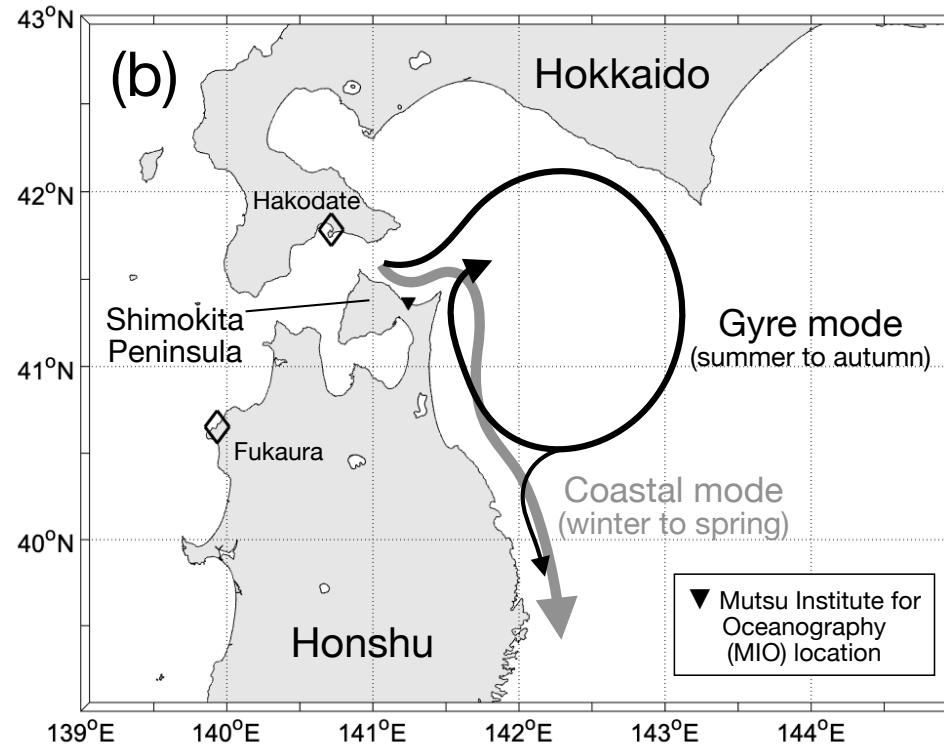
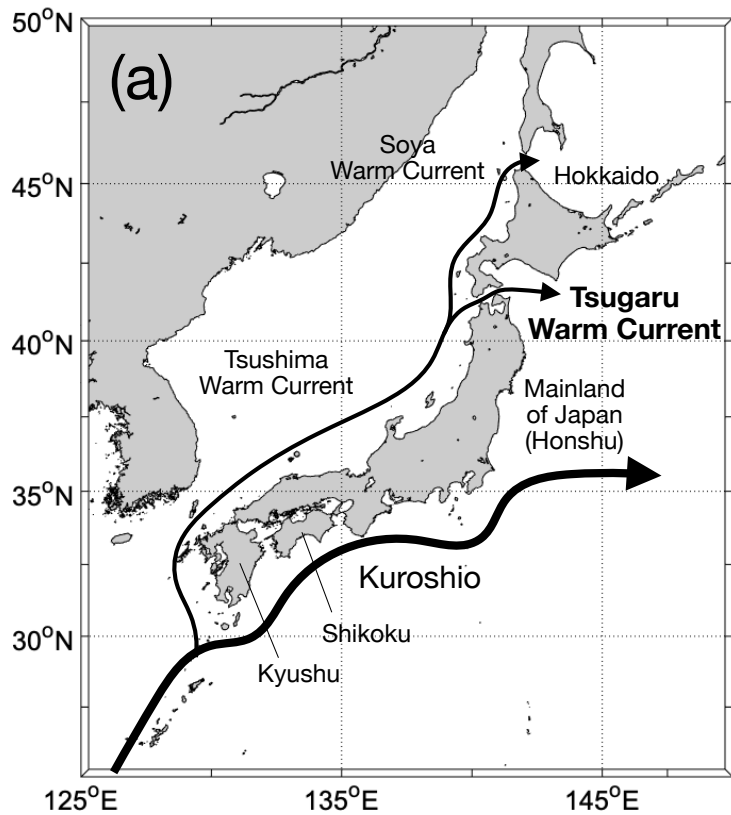


Figure 1. (a) Schematic diagram of the flows around Japan. (b) Seasonal flow pattern of the Tsugaru Warm Current. (c) Observation site of the present study and distribution of the temporal mean velocity at each grid point. The square grids in (c) indicate the bins used to calculate the zonal average of the zonal velocity.

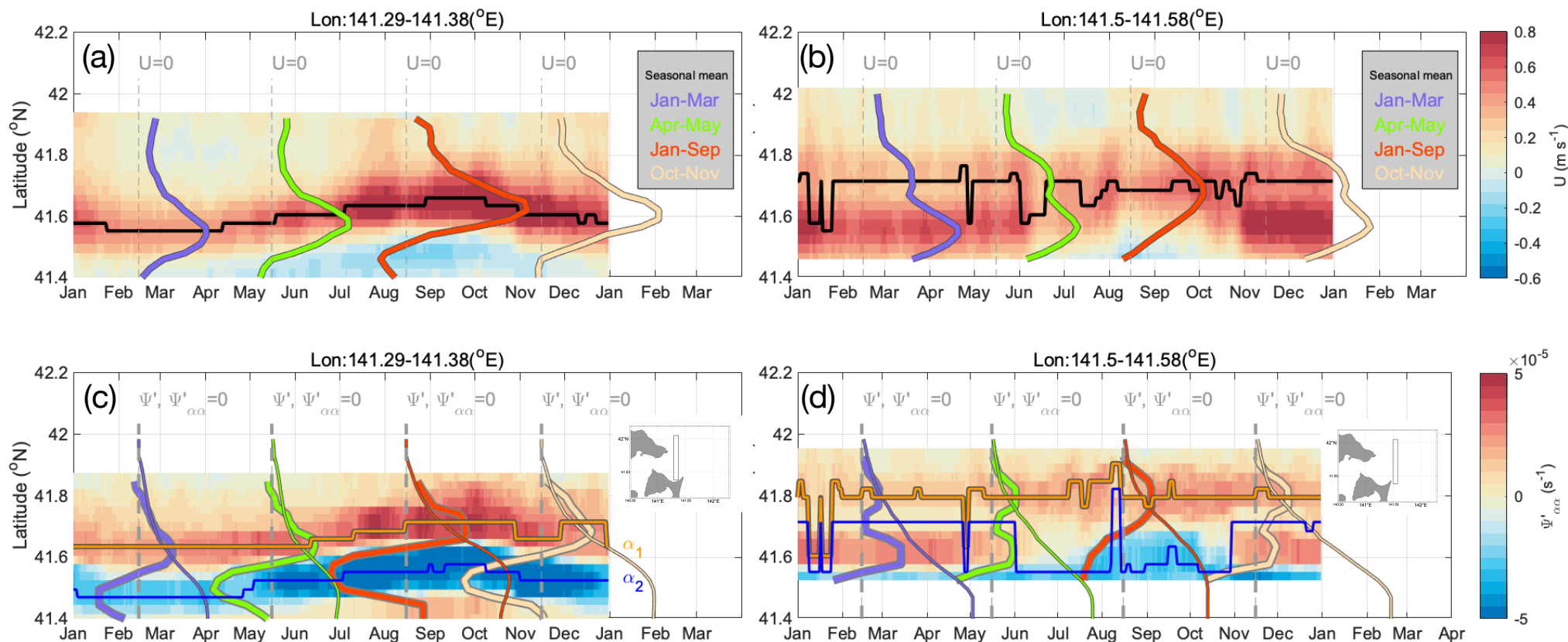


Figure 2. Examples of date–latitude plots of (a) and (b) zonal velocity, and (c) and (d) ψ' (thin lines) and $\psi'_{\alpha\alpha}$ (color and thick lines). The left (right) column denotes Region-a (Region-b). The black line in (a) and (b) denotes the latitude of the jet axis. The orange (blue) line in (c) and (d) denotes the latitude of the maximum (minimum) of $\psi'_{\alpha\alpha}$. See text for definitions of ψ' and $\psi'_{\alpha\alpha}$.

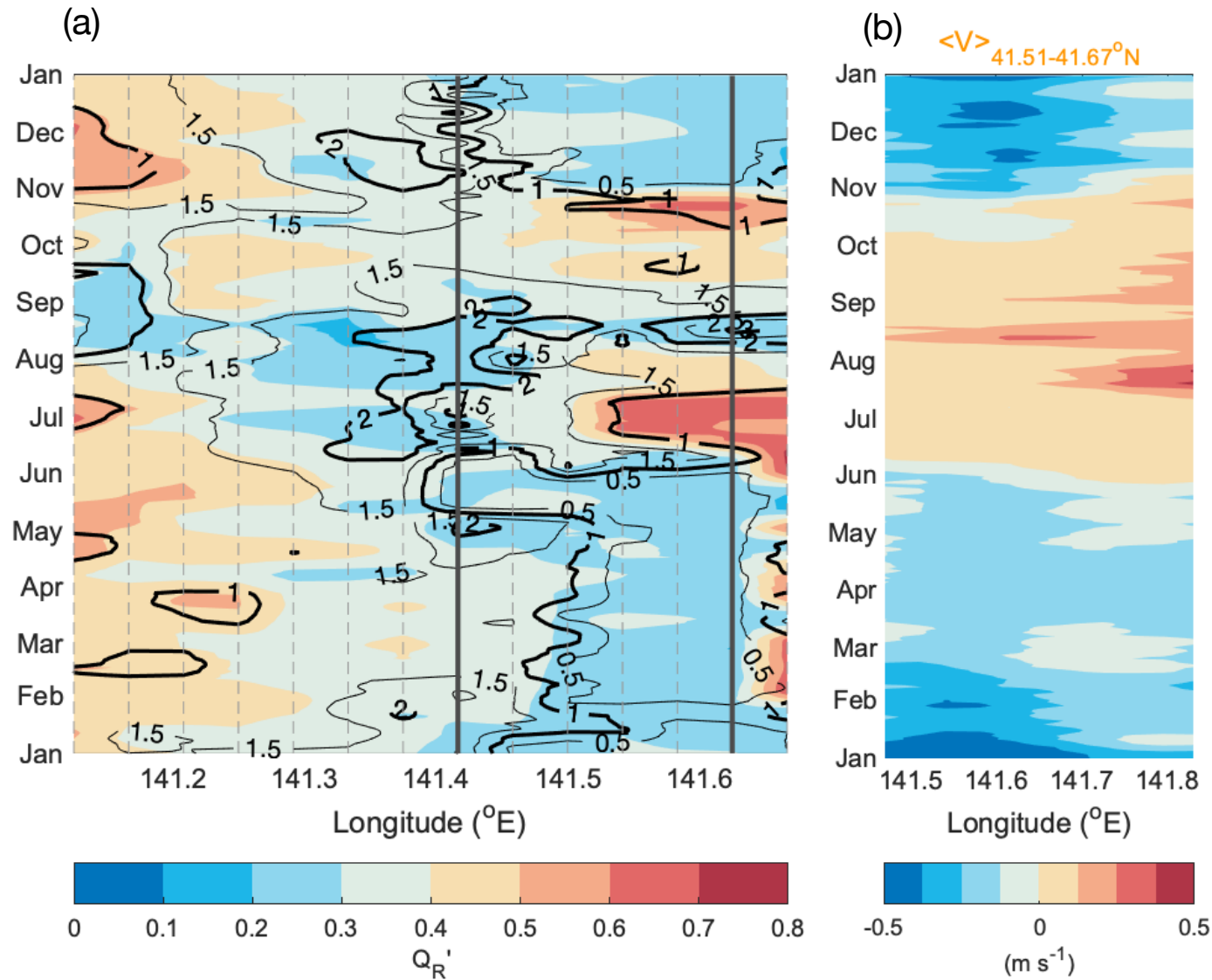


Figure 3. Longitude–date plot of (a) Q_R' (color) and P'/h_0' (contours), and (b) meridional velocity averaged in north–south band. See text for definitions of Q_R' , P' , and h_0' .

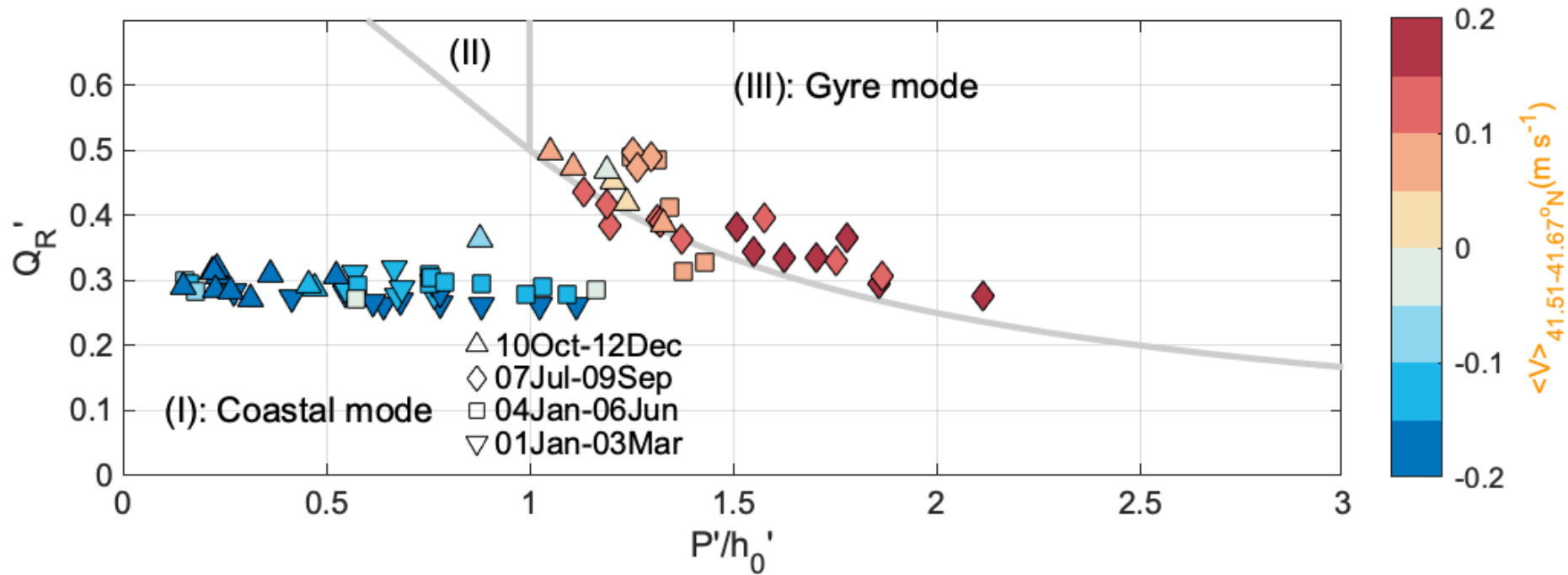


Figure 4. A diagnosis diagram of the flow pattern.